Development of Infrared Imaging Video Bolometer for the ADITYA Tokamak*)

Santosh P. PANDYA, Shwetang N. PANDYA, Zubin SHAIKH, Shamsuddin SHAIKH, Jagannathan GOVINDARAJAN and ADITYA Team

Institute for Plasma Research, Bhat Village, Gandhinagar-382428, India

(Received 10 December 2011 / Accepted 7 May 2012)

The Infrared Imaging Video Bolometer (IRVB) is one of the modern plasma imaging diagnostics which provides the measurement of the temporally as well as spatially resolved (2-D/3-D) power profile radiated from plasma devices. The technique has successfully been tested on a large size tokamak (JT-60U) and the same technique is for the first time being utilized for the medium size tokamak ADITYA (R = 75 cm, a = 25 cm, I_p = 80 kA, $T_e(0) \sim 350$ eV, $\langle N_e \rangle \sim 1.5 \times 10^{13}$ cm^3, B_T = 0.7 T), where the plasma shot duration is ~100 ms and radiated power brightness level is ~2 W/cm^2. The diagnostic is utilizing a 6.4 cm × 6.4 cm size and 2.5 μm thick, free standing Platinum foil. A square aperture 0.7 × 0.7 cm^2 of pinhole camera geometry can provide 9 × 9 bolometer pixel arrays (81 channels) and ~7 cm of spatial resolution at plasma mid-plane with a 45° × 45° wide field of view. This wide field of view covers two semi-tangential views, on either side of the radial view in the tokamak along with a poloidal view. A medium wave infrared camera having 320 × 240 focal plane array, 200 Hz frame rate, noise equivalent temperature difference ~20 mK is used and 10 ms of optimal temporal resolution is experimentally achieved. The present paper discusses the design, development and calibration of the system. The performance of the IRVB system for its time response is experimentally investigated and has also been reported here.

Keywords: infrared imaging video bolometer, bolometry, plasma diagnostic, tokamak, total radiated power loss

DOI: 10.1585/pfr.7.2402089

1. Introduction

Measurement of the radiation power loss from the magnetically confined plasma is important for determination of the power balance study, estimation of energy confinement time, total impurity content, total heat load on the machine wall of the device, observing MARFE and studying how the enhanced impurity radiation leads to MHD unstable configuration. Bolometer is the important diagnostic tool to measure radiation power loss from plasma devices [1–9]. Standard types of bolometer used for the measurement of radiated power from plasma devices are metal foil resistive bolometers [7], AXUV diode based bolometers [8], thermopile bolometer and infrared bolometer [9]. The Infrared Imaging Video Bolometer (IRVB) [1–6] is a new type of bolometer which can provide temporally resolved 2D images of the radiated power from plasma devices. The technique is similar to the metal foil resistive bolometer in the sense that it absorbs the total radiated power and charge exchange neutrals by utilizing a thin metal foil but the signal transmission methods are different. In the case of an IRVB, IR-camera located outside the vacuum vessel measures the 2D temperature distribution of a free-standing thin metal foil. The 2D distribution of radiated power can be determined using a suitable heat diffusion algorithm. Figure 1 shows the schematic of IRVB for Aditya tokamak. The IRVB absorbs total radiated power in a wide energy range (X-rays to visible) and optically transmits the signals in the infrared band. Thus it is immune to electromagnetic (EM) noise and also can work under reactor relevant conditions, therefore it is more suitable for steady state high temperature plasma devices and future fusion devices [1–6]. Advantages of the IRVB over standard bolometers, for its capability to work under reactor relevant conditions and electro-magnetic noise have been reported elsewhere [1–3].

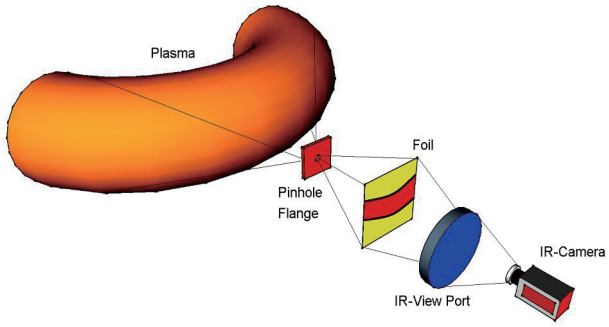

Fig. 1 Schematic diagram of IRVB concept.

author's e-mail: psantosh@ipr.res.in

*) This article is based on the presentation at the 21st International Toki Conference (ITC21).

The IRVB is being successfully operated on the large plasma devices having long plasma discharge and high radiated power levels [1–6]. This technique is being utilized and developed for the first time for a medium-size tokamak ADITYA having a circular limiter with major and minor radii $R = 75\,\text{cm}$ and $a = 25\,\text{cm}$ respectively, typical plasma current $I_p = 80\,\text{kA}$, central electron temperature $T_e(0) = 350\,\text{eV}$, average plasma density $\langle N_e \rangle \sim 1.5 \times 10^{13}\,\text{cm}^3$, toroidal magnetic field at plasma axis $B_T = 0.7\,\text{T}$ and plasma discharge duration $\sim 100\,\text{ms}$. These parameters demand IRVB design to be optimized for higher temporal resolution and sufficiently low Noise Equivalent Power (*NEP*) in order to achieve a high signal to noise ratio (*SNR*). In this paper the work is focused to achieve high *SNR*, high time resolution and wide Field of View (*FOV*). System design, development, calibration and *NEP* is reported in Section 2 to 7. The performance of the IRVB system for its time response is experimentally investigated and also been reported here in Section 8.

2. Design Goals, Consideration and Constrains

IRVB module for ADITYA is designed in accordance with the typical operational parameters and accessibility constraints at the allocated radial port. The design for IRVB diagnostic is based on the required signal level at the foil location considering optimum distances between plasma edge and the IRVB system. Figure 2 shows the poloidal cross-section of Aditya with IRVB diagnostic. The design goals are as follows. Temporal resolution (Δt) $\sim 5\,\text{ms}$, spatial resolution (Δx) $\sim 5\,\text{cm}$, total bolometer channels ~ 100 (10×10 bolometer pixel array), $SNR \geq 50$, FOV $\sim 45° \times 45°$ and broad band absorption of plasma radiation: 6 eV to 8.2 keV.

For the signal estimation in the poloidal cross-section (Fig. 2), typical ohmic heating power is assumed to be $P_{input} \sim 200\,\text{kW}$ and the plasma radiation loss fraction (f) taken from reference [8] ranges from 0.2 to 0.4. Using Eq. (1) the incident power level, ($P_{incident}$) on the center bolometer pixel of the foil is calculated for the different pinhole area ($A_{pinhole}$) and illustrated in Fig. 3 by considering optimum distance from the pinhole to foil ($L_{foil\text{-}pinhole}$), optimum etendue of the system to cover the entire plasma poloidal column, radiation in 4π, plasma volume (V_{plamsa}) and plasma minor radius (a).

$$P_{incident} = \frac{1}{4\pi} \frac{A_{foil\text{-}pixel} A_{pinhole}}{L^2_{foil\text{-}pinhole}} f \frac{P_{input}}{V_{plasma}} 2a \qquad (1)$$

It was found that for the minimum value of f which is 0.2 in the present case and for different pinhole sizes ranging from 5 mm to 10 mm, the corresponding $P_{incident}$ level is ranging from 1 mW to 12 mW.

Based on the different $P_{incident}$ levels the temperature rise (ΔT) with time is analytically calculated for different foil materials using their standard thermal properties,

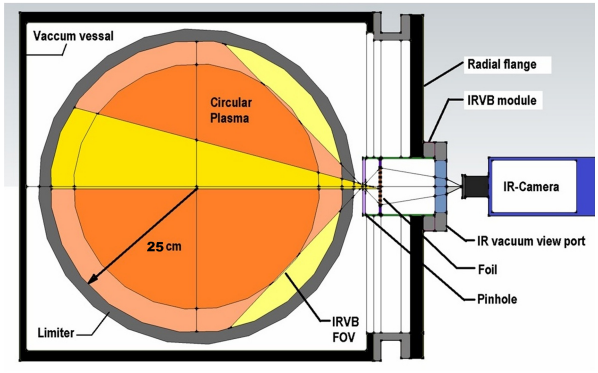

Fig. 2 Poloidal cross-section of ADITYA with IRVB.

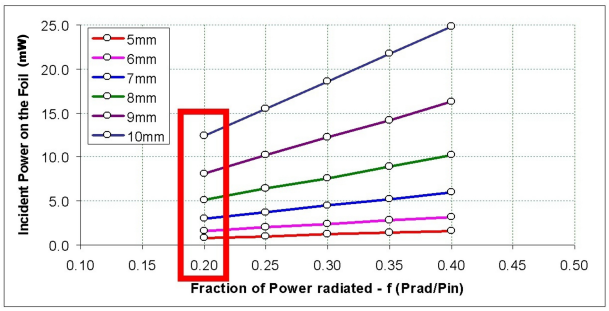

Fig. 3 $P_{incident}$ level at the foil location for different $A_{pinhole}$.

commercially available size and thickness. For 7 mm aperture size, temporal evolution, ΔT, for different foils was found to be well above the Noise Equivalent Temperature Difference (NETD) of an IR-camera ($\sim 0.02°\text{C}$) for time $< 10\,\text{ms}$. It shows that the present design is feasible if the aperture size is $\geq 7\,\text{mm}$.

3. 2-D Signal Estimation on IRVB Foil Area

In order to estimate the signal level at different locations on the IRVB foil and to simulate the expected IRVB image (radiated power brightness, B, in mW/cm^2) on the foil, a basic code is developed which traces the line of sight from each bolometer pixel throughout the plasma volume and calculates the total radiated power at each point in 3-D. By integrating the power along the line, the B falling on the foil area can be estimated. The line radiation from impurity ions is considered as the main source of radiation since it is dominant over other source. Toroidal symmetry is assumed and radial dependence of density and temperature profiles for a circular plasma are calculated using Eqs. (2), (3) where, $T_e(0) = 0.350\,\text{keV}$ and $N_e(0) = 1.5 \times 10^{13}\,\text{cm}^3$. Uniform concentration of impurity ions like iron (0.01%), carbon (3%) and oxygen (3%) is considered throughout the plasma volume and the radial concentration profile is calculated using Eq. (3). The radiative cooling rate (plasma emissivity $g(r)$) at each ra-

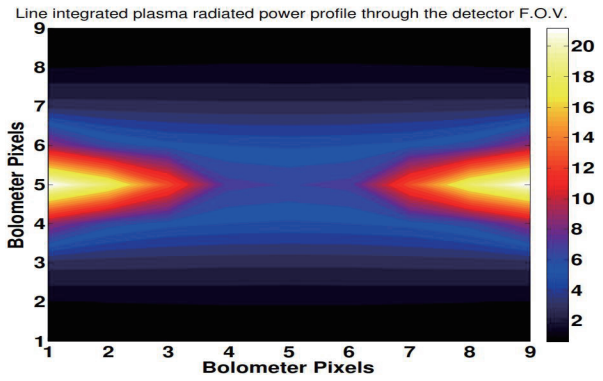

Fig. 4 Simulated IRVB image on foil area.

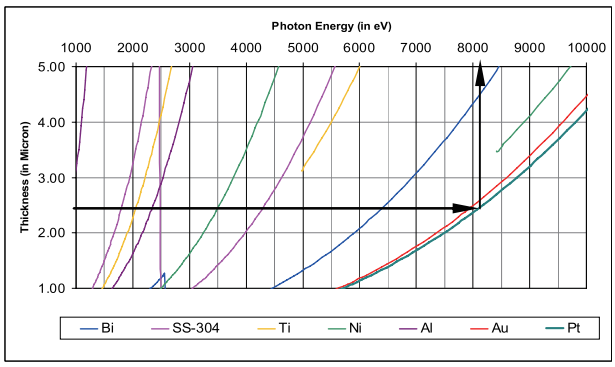

Fig. 5 Photon attenuation thickness for different material.

dial location, Lz, is determined [10] assuming steady state temperature, density profile, coronal equilibrium. $g(r)$ is calculated by substituting Eqs. (2), (3) and Lz in Eq. (4).

$$T_e(r) = T_e(0)\left[1 - \frac{r^2}{a^2}\right]^{1.0} \tag{2}$$

$$N_{e,z}(r) = N_{e,z}(0)\left[1 - \frac{r^2}{a^2}\right]^{1.5} \tag{3}$$

$$g(r) = \sum_Z N_e(r) N_z(r) L_z((T_e(r)) \tag{4}$$

By integrating $g(r)$ for each pixel line of sight, B is calculated for every bolometer channel using Eq. (5)

$$B(x,y) = \sum_l g(r) \cdot dl \tag{5}$$

Finally, using the etendue (ε) for each pixel location the power incident on the foil is calculated using Eq. (6) and expected IRVB image on the foil is simulated as shown in Fig. 4.

$$P_{\text{incident}}(x,y) = \varepsilon B(x,y) \tag{6}$$

Figure 4 shows high intensity of P_{incident} at either end of the foil in toroidal direction which corresponds to the line integrated power loss from two semi-tangential views of the plasma and the center column shows the poloidal power loss profile.

4. Selection of Foil Material

Selection of the radiation absorbing foil material depends on the foil thickness, t_f, (since the sensitivity of the IRVB is $\sim 1/t_f$), commercial availability of the foil in required dimensions and thickness. The upper limit of energy absorption as a function of t_f is illustrated for different foil materials in Fig. 5 [11]. The lower limit of energy absorption depends on the reflectivity from foil's plasma facing surface which can be improved by blackening the foil. After graphite coating, the reflectivity of the foil in the visible range has been found to be $< 5\%$. Sensitivity of the different foil material, Pt, Au and Al are experimentally investigated.

It has been found that the 2.5 μm Pt foils provides higher sensitivity as compare to 2.5 μm Au and 0.8 μm Al foils for the same incident power level. Hence Pt is selected as the radiation absorbing foil for the ADITYA IRVB. Maximum photon stopping energy for a Pt foil of 2.5 μm thickness is found to be ~ 8.2 keV.

5. Data Analysis Scheme and Total Radiated Power Measurement

Forward Time Center Space (FTCS), a finite element analysis algorithm [1, 2, 12] is utilized to retrieve the 2-D power distribution from the foil temperature distribution measured by the IR-camera using Eq. (7).

$$\begin{aligned} P_{\text{Rad}}(x,y,t) = t_f k \Bigg\{ l^2 \left[\frac{T(x,y,t) - T(x,y,t-\Delta t)}{\alpha \Delta t}\right] \\ +[4T(x,y) - T(x,y+l) - T(x,y-l) \\ -T(x+l,y) - T(x-l,y)]_{t-\Delta t} \Bigg\} \end{aligned} \tag{7}$$

Total radiated power from the plasma volume can be calculated by Eq. (8) assuming toroidal symmetry and considering the central pixel column on the IRVB foil which covers maximum poloidal cross-section,

$$P_{\text{Total Rad}} = 2\pi R \sum_i l_i^{\text{PM}} B(i) \tag{8}$$

Where R is the major radius, l_i^{PM} is the spatial resolution of *i-th* pixel on the plasma mid-plan and $B(i)$ is the power brightness of the *i-th* pixel.

6. Calibration of the Foil Properties

Calibration of the foil parameters, namely the product of the thermal conductivity (k) & thickness (t_f) and the thermal diffusivity (α) are necessary in order to measure the incident power accurately [1, 2]. The reasons for the non-uniformities are non-uniform thickness of the foil from manufacturing process, non-uniform coating of the graphite layer (to improve the emissivity of the foil IR-camera side) leads to spatial variation of above mentioned parameters. The calibration setup is shown in Fig. 6 which

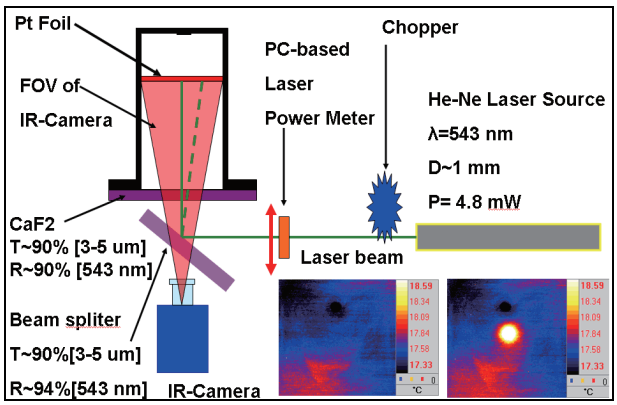

Fig. 6 Schematic diagram of IRVB calibration Setup.

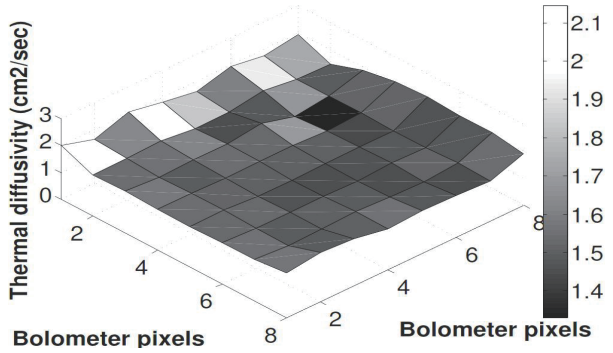

Fig. 7 Spatial variation of thermal diffusivity (α).

can also be used as in-situ calibration when IRVB is installed on a tokamak.

The foil is virtually divided into pixels 2D arrays and then the center of each pixel is irradiated using a He-Ne laser of known power. The laser power is switch-on for 10 seconds and then switched-off. Using and an IR-camera, the temperature rise profile, steady state peak temperature and temperature decay profile is obtained experimentally. The thermal time constant, τ, is calculated using curve fitting on the rise phase and decay phase of the temperature profile, then averaged $\langle\tau\rangle$ is deduced. For each pixel thermal diffusivity, α, (in cm^2/sec) is calculated using the Eq. (9) as shown in Fig. 7.

$$\alpha(x, y) = A_{\text{pix}}/\langle\tau\rangle_{\text{pix}} \tag{9}$$

Where A_{pix} is the virtual pixel area of the foil. In the case of a steady state temperature profile ($dT/dt = 0$), the product of the $k \cdot t_{\text{f}} = \beta$ ((in W/°C) is determined from Eq. (10) as shown in Fig. 8.

$$\beta(x, y) = k. \cdot t_{\text{f}} = P_{\text{laser}}/\Delta T_{\text{peak}}(x, y) \tag{10}$$

Experimentally, it was found that the average α is 6 times greater than theoretical α value of Pt and the average β is 2.5 times greater than the theoretical β value of Pt.

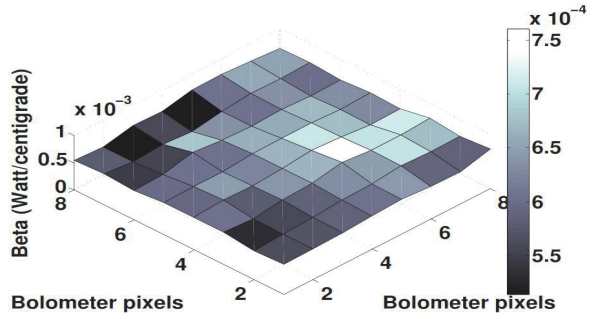

Fig. 8 Spatial variation of $\beta = k \cdot t_{\text{f}}$.

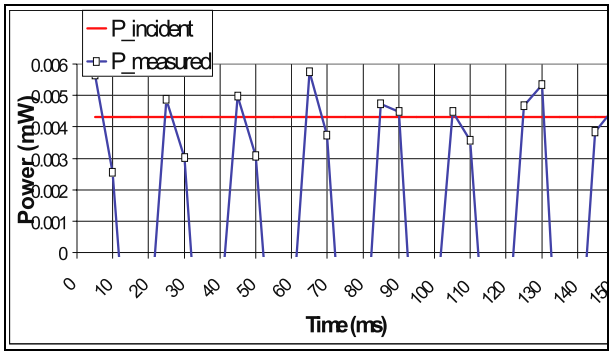

Fig. 9 Power profile determined for square laser pulse heating of 10 ms flat top.

7. Noise Equivalent Power (*NEP*) and Noise Equivalent Power Density (*NEPD*) of IRVB

The *NEP* and *NEPD* of the IRVB are calculated from the following Eqs. (11), (12) [1] where, $k \cdot t_{\text{f}} = 6 \times 10^{-4}$ W/°C, $T_{\text{IR-viewport}} \sim 0.85$ is the transmission of the IR vacuum view port, $\sigma_{\text{IR}} = 0.020$°C is the *NETD* of the IR-camera, $m = 1$ the number of frame to be averaged, $N_{\text{IR}} = 400$ the number of IR-camera pixels covered by one bolometer pixel, $A_{\text{pix}} = 0.49\,\text{cm}^2$, $\alpha = 1.6\,\text{cm}^2/\text{s}$.

$$NEP = 2\sqrt{2} \cdot k \cdot t_{\text{f}} \cdot \frac{1}{T_{\text{IR-viewport}}} \frac{\sigma_{\text{IR}}}{\sqrt{mN_{\text{IR}}}} \times \left[\frac{1}{2}\frac{A_{\text{pix}}}{\alpha}\frac{1}{m\Delta t} + 1\right] \tag{11}$$

$$NEPD = NEP/A_{\text{pix}} \tag{12}$$

NEP and *NEPD* are found to be 50 μW and 100 μW/cm^2 respectively.

8. Experimental Investigation of the IRVB Time Response

The IRVB time response is also experimentally studied by exposing the foil to square wave laser pulses with different flattop (heating time) and then the FTCS is applied on the temperature pulse data. Figure 9 shows the IRVB response to 10 ms laser pulse heating, at 4.5 mW incident power and the power profile is reproduce exper-

imentally.

9. Conclusion

IRVB for ADITYA tokamak is designed, developed, calibrated and tested for its time response. A wide field of view covers two semi-tangential views in the toroidal directions and centre pixel column covers polodial direction. Final ADITYA IRVB parameters are as follows: temporal resolution (Δt) 10 ms, spatial resolution (at plasma mid-plan) ~ 7 cm, *NEP* $\sim 200\,\mu$W, *NEPD* $\sim 400\,\mu$W/cm^2 (experimentally achieved), the *SNR* ranges from 20 to 30, IRVB *FOV* $45^\circ \times 45^\circ$, total spatial channels 81, Pt foil dimension $6.4\,\text{cm} \times 6.4\,\text{cm}$ radiated power absorption in broad band ~ 8.2 keV to 6 eV. From the above parameters it can be concluded that this diagnostic is feasible for the ADITYA tokamak even though it is not meeting all the design goals laid down in Section 2. The shortfalls are mainly due to the space constraints and ADITYA operation parameters.

[1] B.J. Peterson, Rev. Sci. Instrum. **71**, 10, 3696 (2000).
[2] B.J. Peterson *et al.*, Rev. Sci. Instrum. **72**, 1, 923 (2001).
[3] B.J. Peterson *et al.*, Rev. Sci. Instrum. **79**, 10E301 (2008).
[4] N. Ashikawa *et al.*, J. Nucl. Mater. **313**-**316**, 1103 (2003).
[5] B.J. Peterson *et al.*, J. Nucl. Mater. **363**-**365**, 412 (2007).
[6] B.J. Peterson *et al.*, Plasma Fusion Res. **2**, S1018 (2007).
[7] E.R. Muller *et al.*, J. Appl. Phys. **55**, 7, 2635 (1984).
[8] K. Tahiliani *et al.*, Plasma Phys. Control. Fusion **51**, 085004 (2009).
[9] J.C. Ingraham *et al.*, Rev. Sci. Instrum. **54**, 6, 673 (1983).
[10] D.E. Post *et al.*, Atomic Data and Nuclear Data Tables **20**, 5, 397 (1977).
[11] http://henke.lbl.gov/optical_constants/atten2.html
[12] W.H. Press *et al.*, *Numerical Recipes, the Art of Scientific Computing* (Cambridge University Press, Cambridge, 1986) p.635.